Check for updates

ADVANCED ELECTRONIC MATERIALS
www.advelectronicmat.de

Charge Carrier Mobility in Organic Mixed Ionic–Electronic Conductors by the Electrolyte-Gated van der Pauw Method

*Filippo Bonafè, Francesco Decataldo, Beatrice Fraboni, and Tobias Cramer**

Organic mixed ionic–electronic conductors (OMIECs) combine electronic semiconductor functionality with ionic conductivity, biocompatibility, and electrochemical stability in water and are currently investigated as the active material in devices for bioelectronics, neuromorphic computing, as well as energy conversion and storage. Operation speed of such devices depends on fast electronic transport in OMIECs. However, due to contact resistance problems, reliable measurements of electronic mobility are difficult to achieve in this class of materials. To address the problem, the electrolyte-gated van der Pauw (EgVDP) method is introduced for the simple and accurate determination of the electrical characteristics of OMIEC thin films, independent of contact effects. The technique is applied to the most widespread OMIEC blend, poly(3,4-ethylenedioxythiophene) doped with poly(styrenesulfonic acid) (PEDOT:PSS). By comparing with organic electrochemical transistor (OECT) measurements, it is found that gate voltage dependent contact resistance effects lead to systematic errors in OECT based transport characterization. These observations confirm that a contact-independent technique is crucial for the proper characterization of OMIECs, and the EgVDP method reveals to be a simple, elegant, but effective technique for this scope.

1. Introduction

Conjugated polymer:electrolyte blends are fascinating composites that rely on a delocalized π-electron system along the conjugated polymer backbone and an electrolyte acting as an ionic dopant to introduce mobile electronic charges.[1] The most widespread blend is composed by poly(3,4-ethylenedioxythiophene) doped with poly(styrenesulfonic acid) (PEDOT:PSS).[2] PEDOT:PSS finds wide application in several electronic devices ranging from chemical and biological sensors[3,4] to printed circuits[5] and solar cells due to its high conductivity, good chemical stability and facile processing properties. The nano phase separated structure of conjugated polymer:electrolyte blends, gives rise to percolating pathways for ionic as well as electronic carriers and accordingly such blends are termed organic mixed ionic and electronic conductors (OMIECs). Currently, there is a large interest in optimizing the mixed charge transport properties of OMIECs in order to achieve novel and optimized materials for bioelectronic devices such as low-impedance soft electrodes[6,7] organic electrochemical transistors (OECTs) or neuromorphic circuits.[8] At the same time, the mixed conductivity renders the experimental characterization of individual ionic or electronic carrier mobilities difficult as both processes are intrinsically entangled and both can lead to the screening of electric fields or introduce local contact resistances.[9,10] Progress on all fronts is predicated on an advance in understanding the interrelations between ionic transport, electronic transport and ionic–electronic coupling and their dependence on processing, synthetic structure, microstructure/morphology, and electrolyte choice.[11] The extraction of the charge carrier mobility is crucial for the analysis of the transport properties of OMIECs. High-mobility values allow fast device operation and amplified transduction as needed in many applications.[12] Novel methods to characterize carrier mobilities reducing possible artifacts are highly wanted to promote the understanding of OMIECs transport physics and to achieve a rational optimization of this class of materials.

Typical measurements of the electronic mobility of OMIECs are conducted in an electrolyte gated transistor geometry called OECT. OECTs make use of ions injected from an electrolyte to change the doping state and hence the electrical conductivity of the OMIEC semiconducting channel, patterned between the source and drain contacts.[13] These ions are driven by the voltage applied via a gate electrode immersed in the electrolyte, while the source-drain current, flowing in the channel, represents the electrical output.[14] OECT signal transduction is investigated by means of the transfer curves, which highlight the dependence of drain current on gate voltage. The derivative of the transfer curve is the transconductance, g_m, a figure-of-merit describing transduction efficiency. The volumetric capacitance in OMIECs combined with a high electronic mobility endows these devices with very high g_m values.[15]

F. Bonafè, Dr. F. Decataldo, Prof. B. Fraboni, Prof. T. Cramer
Department of Physics and Astronomy
University of Bologna
Viale Berti Pichat 6/2, Bologna 40127, Italy
E-mail: tobias.cramer@unibo.it

The ORCID identification number(s) for the author(s) of this article can be found under https://doi.org/10.1002/aelm.202100086.

© 2021 The Authors. Advanced Electronic Materials published by Wiley-VCH GmbH. This is an open access article under the terms of the Creative Commons Attribution License, which permits use, distribution and reproduction in any medium, provided the original work is properly cited.

DOI: 10.1002/aelm.202100086

Despite OECTs are studied in a wide range of applications, the interpretation of their characteristic curves and the extraction of the figures of merit still represent a difficult challenge. Experiments show that OECT transconductance has a non-monotonic dependence on gate voltage, decreasing at both high and low gate voltages.[16] This behavior is an ubiquitous property of OECTs, reported in devices exploiting different organic semiconductors[13–17] having various electrode geometries[18] and realized using a wide range of fabrication technologies.[19,20] However, existing OECT models do not predict this effect. For example, Bernards' model[14] predicts that transconductance is constant in the linear regime and decreases linearly with gate voltage in the saturation regime. Contact resistance effects can be a possible cause of this behavior.[20] Paterson et al. measured a contact resistance dependency on the gate voltage in n-type OECTs via transmission line measurements.[21] A similar result was obtained by Kaphle et al. for PEDOT:PSS-based OECTs working in depletion mode.[22] This effect was interpreted as the consequence of ion accumulation at the drain contact caused by lateral ion currents in the OECT channel, which were included in a finite element simulation.[9]

Gate-dependent contact effects are typically observed also in normal thin film transistors (TFTs) based on organic semiconductors.[23] A contact-independent technique was developed by Rolin et al. for a more accurate characterization of organic field-effect transistors (OFETs) and was called the gated van der Pauw (gVDP) method.[12] It is based on the normal van der Pauw (VDP) method that is a geometry-independent four-contact electrical measurement widely used to evaluate the sheet conductance σ_s of thin continuous films.[24] In gVDP characterization, a common gate is used to modulate the charge density in VDP devices. gVDP characteristics can be interpreted with a simple model, allowing for the extraction of charge carrier mobility and threshold voltage V_t, as performed by Rolin et al.[12] on several materials. Afterward, Jiang et al. generalized the gVDP method to probe Coulomb interactions on charge transport in few-layer organic crystalline semiconductors.[25] The gating of conjugated polymers immersed in an aqueous electrolyte was observed by Wang et al. in P3HT-based van der Pauw structures.[26]

Here we adapt the electrolyte-gated van der Pauw method to characterize electronic carrier transport in OMIECs. PEDOT:PSS thin films are used as a widely applied model system for OMIECs. We introduce control of the electrolyte gate potential by a potentiostat and measure the sheet conductance in four-point probe geometry as a function of gate potential. We show then for the electrolyte gated van der Pauw method (EgVDP) a simple analysis to extract the threshold voltage V_t and the hole mobility μ_p. Results are compared with two-point probe measurements done in OECT devices, where a simple model is discussed for the quantification of contact resistance effects. The reproducibility of the EgVDP method, combined with its intrinsic independence from contact resistance effects and the straightforward data analysis, validates this technique as an effective strategy for the accurate characterization of electronic mobility in OMIEC thin films.

2. Results

The microstructured PEDOT:PSS thin film devices resulting from the fabrication procedure described in the Experimental Section are shown in **Figure 1**a,b. The optical micrographs demonstrate the well-defined gold contacts serving as electrodes for the measurements. The area covered by PEDOT:PSS gets visible by its slightly blue color. Four symmetric gold electrodes are placed at the edges of the PEDOT:PSS thin film for EgVDP measurements (Figure 1a). As required by VDP's method, the

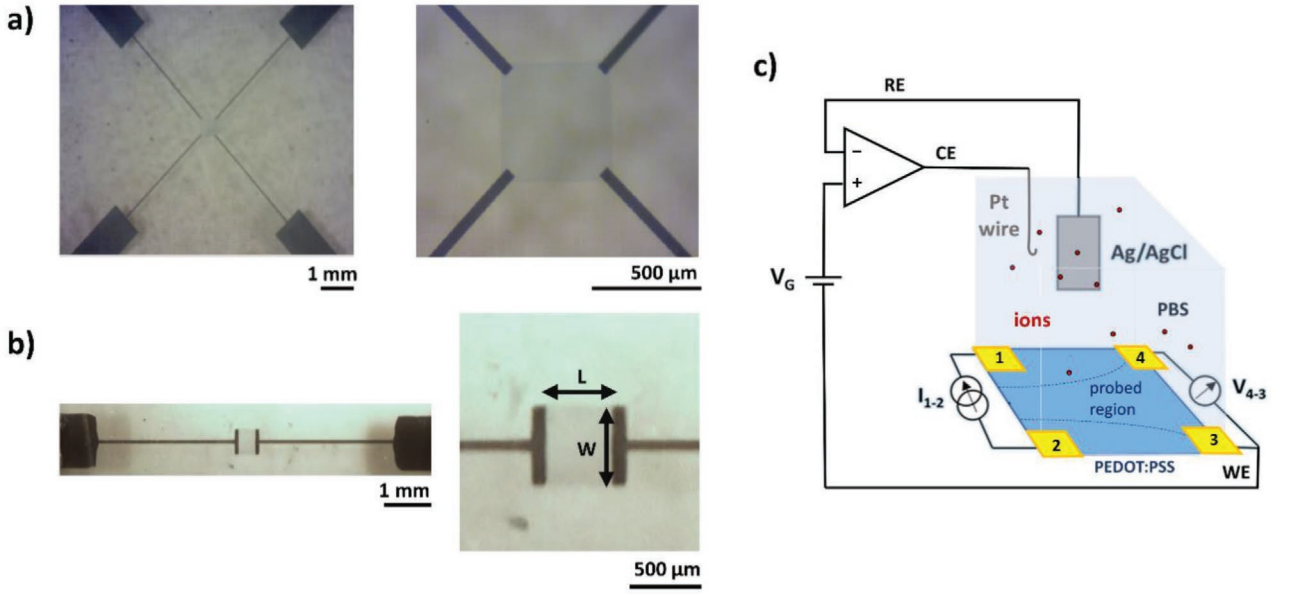

Figure 1. Experimental setup for electrolyte gated van der Pauw measurements to characterize electronic transport in PEDOT:PSS thin films. a) Optical micrographs of a four-contact measurement structure with the PEDOT:PSS active layer patterned at the center of the device. b) Optical micrographs of an organic electrochemical transistor. c) Schematic of the experimental setup for EgVDP characterization.

© 2021 The Authors. Advanced Electronic Materials published by Wiley-VCH GmbH

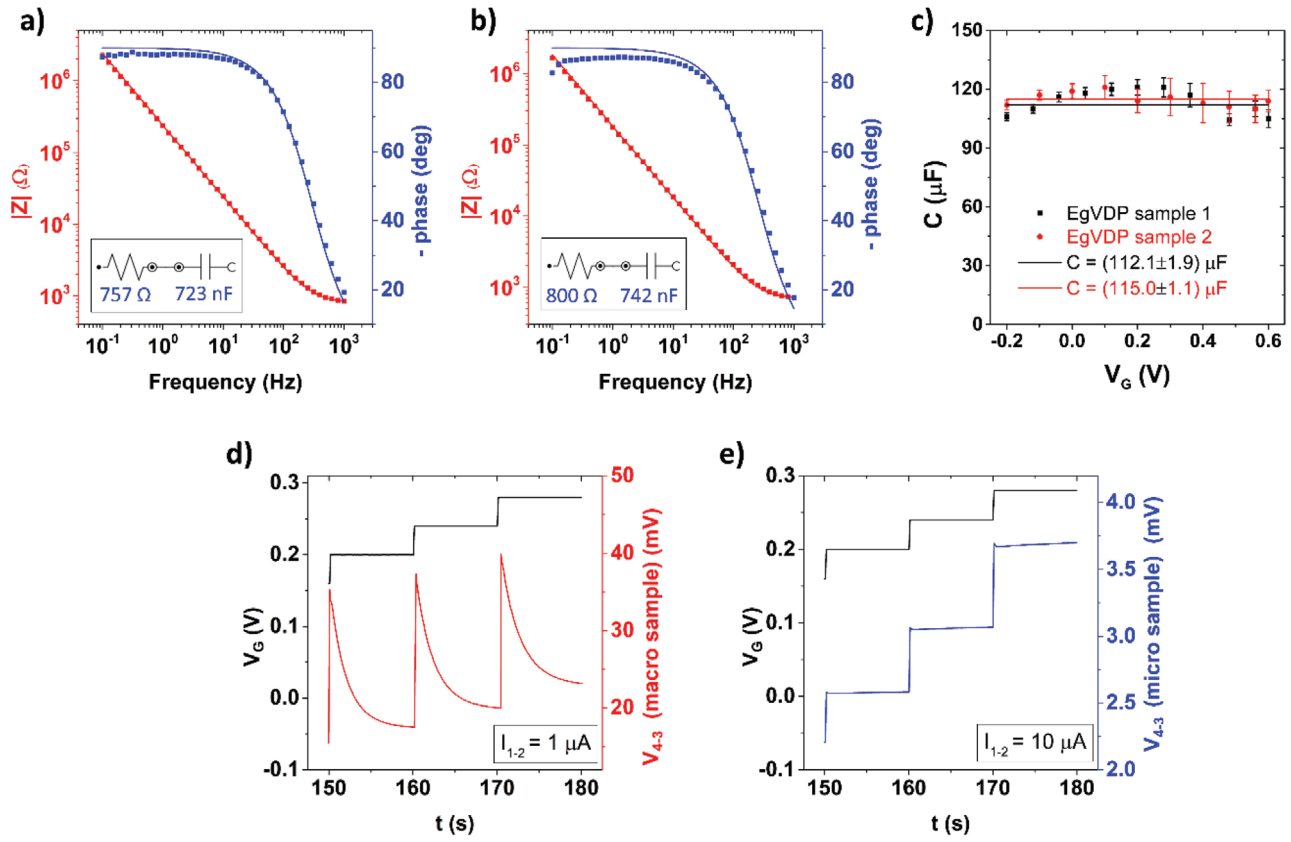

Figure 2. Electrical characterization of electrolyte-gated PEDOT:PSS thin films. Electrochemical impedance spectroscopy of OECT a) four-contact and b) two-contact structures. The Bode plot was fitted with the circuit shown in the inset. The values obtained for the capacitance are shown in c) for different potentials applied to the OECT gate. Time response of d) macroscopic and e) microscopic four-contact structures during electrolyte gated van der Pauw measurements. The voltage drop on the sample between the sensing contacts 4 and 3 is measured in time while varying the applied gate voltage V_G.

dimensions of the metallic contacts are maintained as small as possible with respect to the film size. The PEDOT:PSS film is patterned with a square shape in order to reduce contact displacement errors in VDP measurements.[27] The PEDOT:PSS layer is designed with the same dimensions in two-contact OECTs (Figure 1b). Here, the metallic contacts are patterned with the same width of the PEDOT:PSS film to provide well defined dimensions to the semiconducting channel undergoing electrical measurements.

A schematic of the experimental setup realized for EgVDP characterization is reported in Figure 1c. The PEDOT:PSS active layer is immersed in an electrolyte (PBS 0.1 M). A current is injected between the high-force and the low-force contacts of the device (contacts 1 and 2 in Figure 1c, respectively) and the corresponding voltage drop is measured between the other two (the high and low-sense, contacts 4 and 3, respectively). Simultaneously, a potentiostat is employed to generate an electrical potential (the gating voltage V_G) between an Ag/AgCl reference electrode (RE) and the low-sense contact.

We measured the channel capacitance of the fabricated thin films by characterizing the PEDOT:PSS–electrolyte interface with electrochemical impedance spectroscopy (EIS). Results for EgVDP devices and OECTs are presented, respectively, in **Figure 2**a,b. The acquired Bode plots were fitted with the equivalent circuit shown in the inset. Both interfaces can be modeled with a simple R_C circuit, representing the electrolyte resistance R_{el} and the channel capacitance C of the device.[14] As expected, the frequency response of EgVDP devices reproduces the one of OECTs, since the PEDOT:PSS layers under investigation have the same dimensions. The resulting average volumetric capacitance of PEDOT:PSS is (29 ± 2) F cm^{-3}, which is consistent with literature values.[28] The channel capacitance was measured as a function of the gate voltage (Figure 2c) for two different macroscopic EgVDP devices, with an active PEDOT:PSS film area of 35 mm^2. C resulted to be independent from V_G and approximately constant in the voltage range in which the EgVDP characterizations were performed (–0.2 V < V_G < 0.6 V). Therefore, measurements were fitted with a constant line, and the resulting mean capacitances are compatible to each other.

Next we investigate the timescales at which gating is effective in electrolyte-gated van der Pauw structures. Figure 2d,e shows the behavior of two EgVDP structures with different dimensions when gate voltage steps are applied. The time response of a larger, macroscopic device (Figure 2d), with an active PEDOT:PSS film area of 35 mm^2, is compared with the one of a microscopic EgVDP structure (Figure 2e), with film area 0.25 mm^2 (see Figure 1a). During each step, V_G is kept constant for 10s, and then increased by 0.04 V (scan rate 4 mV s^{-1}). In both cases, the voltage drop on the sample between the sensing contacts 4 and 3 reaches a stationary state

© 2021 The Authors. Advanced Electronic Materials published by Wiley-VCH GmbH

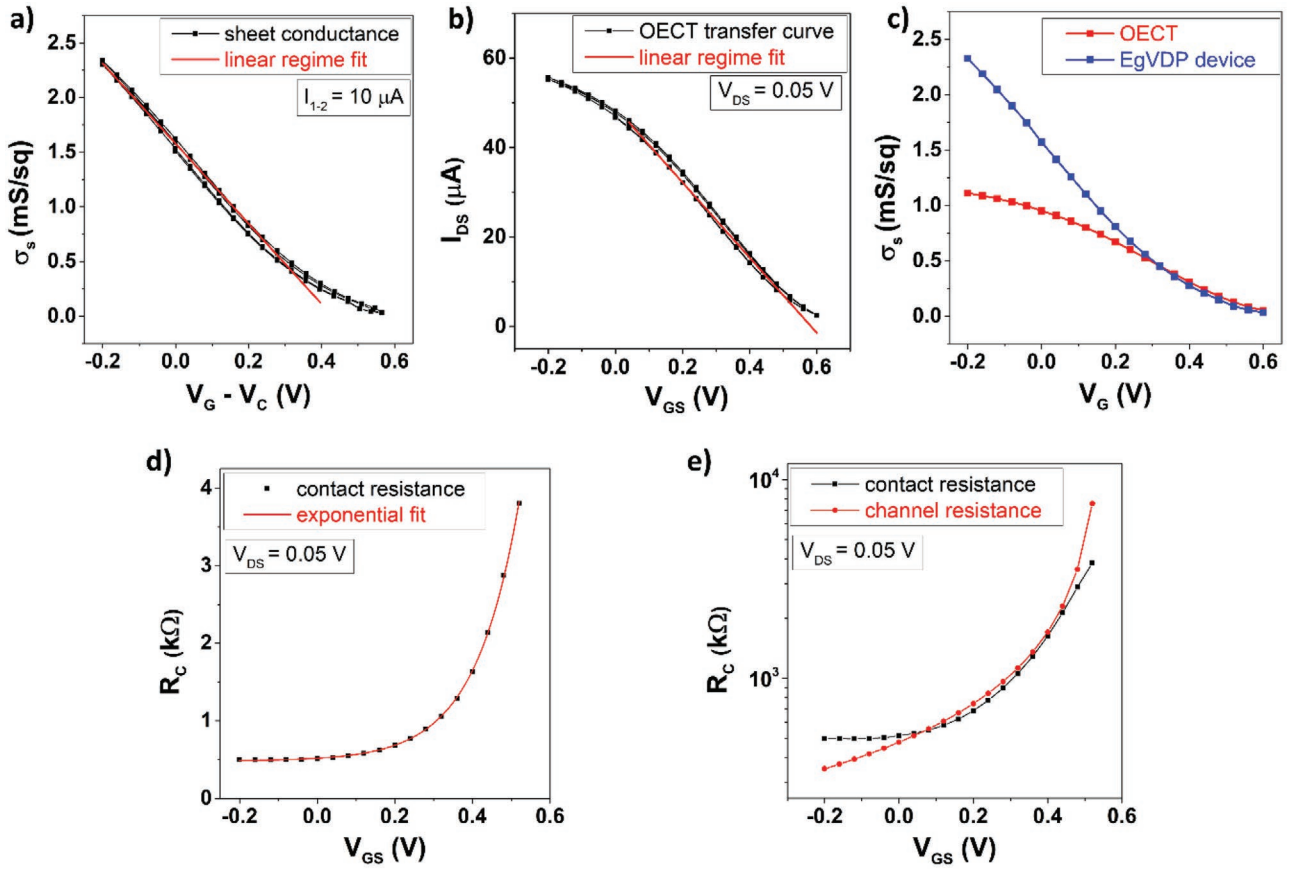

Figure 3. Analysis of the van der Pauw and OECT transport characterizations. a) Sheet conductance of an electrolyte gated van der Pauw structure plotted as a function of $V_G - V_C$ (with $V_C = V_{4-3}/2$). A constant current $I_{1-2} = 10$ µA is injected between the forcing contacts. b) Transfer curve of an OECT. The drain voltage is fixed at 0.05 V. The linear regime of the EgVDP and OECT characteristics is fitted to extract the mobility and the threshold voltage. c) Comparison between the sheet conductance of an EgVDP (red line) and an OECT (blue line). d) Evaluation and exponential fit of the contact resistance as a function of the gate voltage in an OECT. e) Comparison between the contact resistance and the channel resistance of an OECT device at different gate voltages.

after a transient R_C response. The time duration of the transitory state depends on the time constant of the device (τ), which is proportional to its capacitance. Many studies demonstrate that the electrical capacitance of a PEDOT:PSS film depends on its volume.[29] As the polymeric layers present the same film thickness in macroscopic and microscopic devices, the difference in capacitance is only related to the different film area. Figure 2d demonstrates that the large capacitance of macroscopic EgVDP samples poses a strong limitation during the EgVDP characterization. In particular, when the carrier concentration in PEDOT:PSS is small (high channel resistance), the charge/discharge processes are too slow for a reasonable scan rate on V_G and the circuit fails to reach the stationary behavior. For this reason, during the characterization of macroscopic sized samples it was not possible to apply gating voltages above 0.4 V, and only a limited range of carrier concentration was studied. Miniaturization is therefore crucial to study low carrier concentration regimes.

The results of the electrolyte gated transport measurements are reported in **Figure 3**a,b. The gate voltage is scanned between −0.2 and 0.6 V (forward and backward scans), while a constant current $I_{1-2} = 10$ µA is injected between the High and Low force contacts 1 and 2. The gate potential range of the experiment was selected to avoid material degradation and water splitting processes. The measured sheet conductance of the thin film (Figure 3a) is plotted as a function of the difference between V_G and V_C, with V_C being defined as half the voltage drop measured on the sample ($V_C = V_{4-3}/2$). For comparison, the transfer curve of a two-contact OECT measured in linear regime ($V_{DS} =$ 0.05 V) is presented in Figure 3b. In both cases, the behaviors of the samples are reproducible during the gate voltage scan, and measurements show only a small hysteresis. Both EgVDP devices and OECTs reach a linear operation regime below a threshold voltage V_t. The linear behavior of an OECT is commonly described by the Bernard's model[14]

$$I_{DS} = \mu_p C \frac{W}{L}\left(V_t - V_{GS} + \frac{V_{DS}}{2}\right)V_{DS} \quad (1)$$

Where C indicates the capacitance per unit area of the PEDOT:PSS–electrolyte interface, and W, L are respectively the channel width and length. Equation (1) can also be used to describe EgVDP operation. The probed region between the sensing contacts 4 and 3 in EgVDP structures can be treated

© 2021 The Authors. Advanced Electronic Materials published by Wiley-VCH GmbH

Table 1. PEDOT:PSS mobilities and threshold voltages measured from EgVDP and OECT characterization.

Sample	μ_p [cm^2 V^{-1} s^{-1}]	V_t [V]
EgVDP 1	12.0 ± 0.5	0.436 ± 0.011
EgVDP 2	11.7 ± 0.4	0.44 ± 0.02
EgVDP 3	11.3 ± 0.4	0.45 ± 0.02
OECT 1	5.9 ± 0.3	0.57 ± 0.02
OECT 2	6.7 ± 0.2	0.520 ± 0.012
OECT 3	4.2 ± 0.2	0.530 ± 0.010

as a semiconducting channel with source and drain at potentials V_3 and V_4, respectively. The geometrical dimensions of the channel are related by $L/W = \ln(2)/\pi$, as demonstrated by van der Pauw for square VDP structures.[24] The injected current I_{1-2} can be expressed in terms of the sheet conductance σ_s as

$$\frac{\ln(2)}{\pi} I_{1-2} = \sigma_s |V_{4-3}| \tag{2}$$

with

$$\sigma_s = \mu_p C|V_t - V_G + V_C| \tag{3}$$

The space charge density accumulated in the PEDOT:PSS layer is $\delta = C|V_t - V_G + V_C|$, where $V_C = V_{4-3}/2$ approximates the potential in the probed region of the EgVDP structures.

Figure 3a,b was fitted with Equations (3) and (1), respectively to extract the charge carrier mobility and the threshold voltage of the devices. Quantitative results obtained from different samples are reported in **Table 1**.

The mobilities measured in OECT devices are in good comparison with findings described in literature. Typically values measured in OECTs are on the order of 1–10 cm^2 V^{-1} s^{-1}.[10–15] In general, high mobilities for transport in OECT are reasonable, as the mobility is extracted in the high carrier density regime, were carrier trapping at band-edge states has only limited importance. At the same time, the accumulation does not exceed a critical limit at which energetic and structural disorder set-in due to PEDOT overoxidation.[30] Table 1 also confirms that the EgVDP method allows for a very reproducible parameter extraction on the three different samples. Mobilities measured with the contact-independent EgVDP characterization are systematically higher than the ones measured with OECTs. A similar value for mobility was determined in contact independent measurements based on terahertz and infrared spectroscopy.[31]

In order to compare in detail the difference between the OECT and EgVDP measurement techniques, we compare for both the calculated sheet conductances in Figure 3c. At high gate voltages (low carrier concentrations) both curves are superimposed. Instead at low V_G, the EgVDP measurement shows the linear increase in conductance due to accumulation of carriers, while the two-contact OECT measurement flattens and shows a significantly limited conductance. The difference between the two measurements can only be attributed to contact resistance effects. The presence of a contact resistance R_C generates an additional potential drop along the semiconducting channel of an OECT: $I_{DS} = V_{DS}/(R_{ch} + R_C)$, where R_{ch} indicates the channel resistance

$$R_{ch} = \frac{1}{\mu_p c \frac{W}{L}\left(V_t - V_{GS} + \frac{V_{DS}}{2}\right)} \tag{4}$$

By substituting in the transfer curve equation the contact-independent mobility $\langle\mu_p\rangle = (11.7 \pm 0.3)$ cm^2 V^{-1} s^{-1} (obtained by averaging the EgVDP mobilities), the following equation can be solved to calculate R_C as a function of the gate voltage

$$I_{DS} = \frac{\langle\mu_p\rangle c \frac{W}{L}\left(V_t - V_{GS} + \frac{V_{DS}}{2}\right)}{\langle\mu_p\rangle c \frac{W}{L}\left(V_t - V_{GS} + \frac{V_{DS}}{2}\right) R_c + 1} V_{DS} \tag{5}$$

The results of this analysis are reported in Figure 3d. We thus obtain that, in linear regime, the contact resistance of an OECT is exponentially dependent on the gate voltage, and the equation

$$R_c(V_{GS}) = a * \exp(b * V_{GS}) + c \tag{6}$$

is fitted to the data, obtaining $a = (0.0351 \pm 0.0012)$ V, $b = (8.76 \pm 0.07)$ V^{-1} and $c = (0.483 \pm 0.005)$ V. Hence carrier injection from the contact into the semiconductor channel is strongly mediated by the gate voltage in OECTs. This aspect is clearly visible in Figure 3e, which compares the OECT channel resistance with the contact resistance, both as a function of the gate potential. From this plot it is possible to observe that the gate-dependent contact resistance dominates on the channel resistance at low gate voltages. Consequently, contact resistance effects strongly affect the modulation of the PEDOT:PSS conductivity when the electronic carrier density in the material is high, causing the conductivity saturation typically observed in OECTs. Previous works demonstrate that this effect can lead to mobility underestimations[23–32] consistent with the results of our experiment. In contact-resistance free measurements this effect is not observed and the conductivity of van der Pauw structures increases linearly with negative gate voltages in the potential range of measurements.

A contact resistance exponentially dependent on the gate voltage was already found in OECTs by Kaphle et al.[22] This observation was interpreted as the consequence of ion accumulation at the drain contact, caused by lateral ion currents in the OECT channel.[9] Lateral ion transport can also be responsible for the threshold voltage overestimation in OECT characteristics. According to Kaphle's simulation,[9] the application of a positive drain-to-source voltage ($V_{DS} = 0.05$ V) generates an equilibrium ion distribution in the channel which partially depletes from cations the region nearby the drain contact. Consequently, the electronic conductivity of PEDOT:PSS is locally increased, as the concentration of ionic de-dopants is reduced.[33] This effect can shift the threshold voltage of an OECT working in depletion mode toward higher gate voltages. In the EgVDP such a systematic error in threshold voltage determination cannot occur. A pair of high impedance electrodes measures

© 2021 The Authors. Advanced Electronic Materials published by Wiley-VCH GmbH

the electric field strength relevant for carrier acceleration and is thus not affected by local ion-accumulation. We remark that in our experiment, we used a potentiostat and a well-defined reference electrode (Ag/AgCl 3 M KCl) to have a precise control of the electrochemical potential in both van der Pauw and OECT characteristics. Under such conditions, the threshold voltage is reproducible and can be related the materials properties. Therefore, it is possible to compare the threshold voltages extracted with both techniques. In doing so, we observe that contact resistance affects the linearity of the OECT transfer curves and renders the extraction of V_t difficult. On the other hand, the transfer curves acquired with EgVDP measurements are perfectly linear at high carrier densities, allowing for an accurate determination of the contact-independent threshold voltage. For such an ideal case, one can refer to more advanced models on carrier transport that relate V_t to the energy levels of the semiconductor and work function of the gate terminal (see Figure S1 in the Supporting Information for further details).[34] In particular, V_t results to be dependent on the position of the valence band edge of PEDOT in its pristine state, which electrochemical measurements indicate to be $W_{PEDOT} = 4.5$ eV.[35] The contact independent threshold voltage extracted from EgVDP characterizations allows for a better estimate of this value ($W_{PEDOT,\ EgVDP} = (4.36 \pm 0.04)$ eV) with respect to OECT measurements ($W_{PEDOT,\ OECT} = (4.25 \pm 0.03)$ eV).

Finally, we note that alternative contact-independent techniques such as FPP[16] and transmission line method (TLM)[22] can be used to extract the charge carrier mobility in the high-charge density regime of OMIECs. However, we think that the EgVDP method has many advantages over them[12]: TLM requires multiple devices with different channel length and mobility extraction is weakened by the problematic determination of the threshold voltage.[36] As shown in Figure 3c, transfer curves of OECT are not linear and therefore threshold voltage depends strongly on the mathematical extraction procedure. On the other hand, gated four-point probe (gFPP) devices require the precise alignment of the voltage probes along the very edge of the semiconductor channel, and mobility extraction is typically compromised by small variations in device geometry.[37] In contrast, measuring the EgVDP device is of the same complexity as the gFPP device measurement (both require five contacts). However, the data obtained are more precise than in gFPP thanks to the averaging over different sides and the independence from geometric dimensions.

3. Conclusions

In this paper, we introduce a four-point probe characterization technique for organic mixed OMIECs, the electrolyte-gated van der Pauw's method. This technique is applied for the first time to PEDOT:PSS thin-film devices for an accurate extraction of the mobility and the threshold voltage that are representative of the transport properties of the blend. The EgVDP method combines many advantages: 1) the device structure and fabrication constraints are the same as for standard OECTs, allowing easy device integration and comparison; 2) the method is independent from contact effects that are detrimental to transistor characteristics; 3) a straightforward data analysis allows precise parameter extraction owing to the inherent averaging and independence from geometrical dimensions. We tested this method on three different EgVDP devices, obtaining highly reproducible results. The average PEDOT:PSS mobility and threshold voltage obtained from measurements are $\langle \mu_p \rangle = (11.7 \pm 0.3)$ cm^2 V^{-1} s^{-1} and $\langle V_t \rangle = (0.44 \pm 0.02)$ V. By comparing this result with two-point probe measurements, we found that contact resistance effects complicate the extraction of both the mobility and the threshold voltage, leading to an underestimation and an overestimation for the former and the latter, respectively. These observations indicate that a contact-independent technique is crucial for the proper characterization of PEDOT:PSS, and the EgVDP method is revealed to be a simple, elegant, but effective technique for this scope. Given its general applicability and good accuracy, the EgVDP method can be a promising and useful tool to characterize new semiconducting materials with mixed ionic and electronic conductivity.

4. Experimental Section

Device Fabrication: Both four-contact devices for EgVDP characterization and OECTs were fabricated with photolithography. Glass substrates (25 × 25 mm^2) were cleaned by sonication in distilled water/acetone/isopropanol baths, and then blow dried using nitrogen flux. Afterward, substrates were dehydrated for 10 min at 110 °C. The Microposit S1818 positive photoresist was spin coated (4000 rpm for 10 s) and annealed at 110 °C for 1 min. Metallic contacts were patterned through direct laser lithography by using the ML3 Microwriter (from Durham Magneto Optics). The photoresist was developed with Microposit MF-319 developer. Then, 15 nm of chromium and 20 nm of gold were deposited by thermal evaporation. Samples were immersed in acetone for 4 h for photoresist lift-off, and then rinsed by sonication in acetone/isopropanol/distilled water baths. A double layer of S1818 was deposited and treated for 6 min in chlorobenzene for the photolithography of the PEDOT:PSS channel.[38] After the development, substrates were treated with air plasma (15 W for 2 min) and the PEDOT:PSS solution was spin coated at 3000 rpm for 10 s. The solution was made of 94% PEDOT:PSS (Heraeus, Clevios PH1000) with 5% of ethylene glycol (EG) (Sigma Aldrich), 1% of 3-glycidoxypropyltrimethoxysilane (GOPS), and 0.25% of 4-dodecylbenzenesulfonicacid (DBSA). This suspension was treated in ultrasonic bath for 10 min and filtered using 1.2 µm cellulose acetate filters (Sartorius) before the deposition. The resulting film thickness was (100 ± 10) nm. The samples were subsequently baked at 120 °C for 1 h. Finally, the photoresist was lifted off with the procedure discussed before.

Electrochemical Characterization: Samples were immersed in an electrochemical cell containing PBS (0.1 M). A thin PDMS film prevented the direct contact between the metallic electrodes and the solution. A nitrogen-saturated environment was maintained in the cell during measurements. EIS was performed with the potentiostat Metrohm Autolab PGSTAT204. A sinusoidal wave with 10 mV rms amplitude was generated in the frequency range between 0.1 and 1000 Hz. The Amelchem 373/SSG/12 Ag/AgCl was used as RE, while a platinum wire was used as counter electrode. The device contacts (the working electrode) were short-circuited during measurements.

Electrical Measurements: The four contacts of the EgVDP structures were connected to the Keysight B2912A source-measure unit (SMU) for four-point probe characterization. A current $I_{1-2} = 10$ µA was sourced in contact 1 and drained at contact 2, while the potential difference V_{4-3} between contacts 4 and 3 was measured. The working electrode (WE) of the potentiostat was connected to the Low-sense contact to generate a voltage $V_G = V_{Ag/AgCl} - V_3$. A gate voltage staircase was applied between –0.2 and 0.6 V. During each step, V_G was kept constant for 10 s and then increased (or decreased) by 0.04 V. The potential scan was repeated twice for each characterization, in order to test the reproducibility of the

© 2021 The Authors. Advanced Electronic Materials published by Wiley-VCH GmbH

sample response. For σ_s extraction, $R_{1-2} = |V_{4-3}|/I_{1-2}$, the resistance in the probed region alongside 1–2. The measurement of R_{2-1} along the same side was obtained by reversing the direction of the current. Next, the resistances along the adjacent side of the square (R_{2-3} and R_{3-2}) were measured in the same way, and the four resistance values were averaged as $\langle R \rangle$. Finally, thanks to the fourfold symmetry of the film,[24] the sheet conductance was calculated as $\sigma_s = \frac{\ln(2)}{\pi \langle R \rangle}$. OECTs were characterized by measuring their transfer characteristic. A constant voltage $V_{DS} = 0.05$ V was applied between the drain and the source contacts. The potentiostat generated a gate voltage V_{GS} between the Ag/AgCl RE and the source contact (WE). A V_{GS} staircase was scanned between –0.2 and 0.6 V with the same parameters adopted for EgVDP measurements, and the corresponding drain current I_{DS} was measured with the SMU.

Supporting Information

Supporting Information is available from the Wiley Online Library or from the author.

Acknowledgements

T.C. gratefully acknowledges financial support from the EU Horizon 2020 FETOPEN-2018-2020 program (project "LION-HEARTED," grant agreement no. 828984).

Conflict of Interest

The authors declare no conflict of interest.

Data Availability Statement

The data that support the findings of this study are available from the corresponding author upon reasonable request.

Keywords

charge carrier mobilities, contact resistances, electrolyte gated van der Pauw measurements, organic electrochemical transistors, organic mixed ionic–electronic conductors

Received: January 27, 2021
Revised: June 15, 2021
Published online:

[1] C. Liu, K. Huang, W. T. Park, M. Li, T. Yang, X. Liu, L. Liang, T. Minari, Y. Y. Noh, *Mater. Horiz.* **2017**, *4*, 608.
[2] A. Elschner, S. Kirchmeyer, W. Lövenich, U. Merker, K. Reuter, *PEDOT: Principles and Applications of an Intrinsically Conductive Polyme*CRC Press, Boca Raton, FL **2010**.
[3] F. Decataldo, I. Gualandi, M. Tessarolo, E. Scavetta, B. Fraboni, *APL Mater.* **2020**, *8*, 091103.
[4] I. Gualandi, M. Marzocchi, E. Scavetta, M. Calienni, A. Bonfiglio, B. Fraboni, *J. Mater. Chem. B* **2015**, *3*, 6753.
[5] W. Lee, T. Someya, *Chem. Mater.* **2019**, *17*, 6347.
[6] D. Khodagholy, J. N. Gelinas, T. Thesen, W. Doyle, O. Devinsky, G. G. Malliaras, G. Buzsáki, *Nat. Neurosci.* **2015**, *18*, 310.
[7] A. Campana, T. Cramer, D. T. Simon, M. Berggren, F. Biscarini, *Adv. Mater.* **2014**, *26*, 3874.
[8] H. Ling, D. A. Koutsouras, S. Kazemzadeh, Y. Van De Burgt, F. Yan, P. Gkoupidenis, *Appl. Phys. Rev.* **2020**, *7*, 011307.
[9] V. Kaphle, P. R. Paudel, D. Dahal, R. K. Radha Krishnan, B. Lüssem, *Nat. Commun.* **2020**, *11*, 2515.
[10] F. Mariani, F. Conzuelo, T. Cramer, I. Gualandi, L. Possanzini, M. Tessarolo, B. Fraboni, W. Schuhmann, E. Scavetta, *Small* **2019**, *15*, 1902534.
[11] B. D. Paulsen, K. Tybrandt, E. Stavrinidou, J. Rivnay, *Nat. Mater.* **2020**, *19*, 13
[12] C. Rolin, E. Kang, J. H. Lee, G. Borghs, P. Heremans, J. Genoe, *Nat. Commun.* **2017**, *8*, 14975.
[13] J. Rivnay, S. Inal, A. Salleo, R. M. Owens, M. Berggren, G. G. Malliaras, *Nat. Rev. Mater.* **2018**, *3*, 17086.
[14] D. A. Bernards, G. G. Malliaras, *Adv. Funct. Mater.* **2007**, *17*, 3538.
[15] J. Rivnay, P. Leleux, M. Ferro, M. Sessolo, A. Williamson, D. A. Koutsouras, D. Khodagholy, M. Ramuz, X. Strakosas, R. M. Owens, C. Benar, J. M. Badier, C. Bernard, G. G. Malliaras, *Sci. Adv.* **2015**, *1*, e1400251.
[16] J. T. Friedlein, J. Rivnay, D. H. Dunlap, I. McCulloch, S. E. Shaheen, R. R. McLeod, G. G. Malliaras, *Appl. Phys. Lett.* **2017**, *11*, 023301.
[17] D. Ofer, R. M. Crooks, M. S. Wrighton, *J. Am. Chem. Soc.* **1990**, *112*, 7869.
[18] E. Bihar, Y. Deng, T. Miyake, M. Saadaoui, G. G. Malliaras, M. Rolandi, *Sci. Rep.* **2016**, *6*, 27582.
[19] D. Khodagholy, J. Rivnay, M. Sessolo, M. Gurfinkel, P. Leleux, L. H. Jimison, E. Stavrinidou, T. Herve, S. Sanaur, R. M. Owens, G. G. Malliaras, *Nat. Commun.* **2013**, *4*, 2133.
[20] M. Afonso, J. Morgado, L. Alcácer, *J. Appl. Phys.* **2016**, *120*, 165502.
[21] A. F. Paterson, H. Faber, A. Savva, G. Nikiforidis, M. Gedda, T. C. Hidalgo, X. Chen, I. McCulloch, T. D. Anthopoulos, S. Inal, *Adv. Mater.* **2019**, *31*, 78691902291.
[22] V. Kaphle, S. Liu, A. Al-Shadeedi, C.-M. Keum, B. Lüssem, *Adv. Mater.* **2016**, *28*, 8766.
[23] C. Liu, G. Li, R. Di Pietro, J. Huang, Y. Y. Noh, X. Liu, T. Minari, *Phys. Rev. Appl.* **2017**, *8*, 034020.
[24] L. J. van der Pauw, *Philips Tech. Rev.* **1958**, *20*, 220.
[25] S. Jiang, J. Qian, Q. Wang, Y. Duan, J. Guo, B. Zhang, H. Sun, X. Wang, C. Liu, Y. Shi, Y. Li, *Adv. Electron. Mater.* **2020**, *6*, 2000136.
[26] S. Wang, M. Ha, M. Manno, C. Daniel Frisbie, C. Leighton, *Nat. Commun.* **2012**, *3*, 1210.
[27] D. W. Koon, A. A. Bahl, E. O. Duncan, *Rev. Sci. Instrum.* **1989**, *60*, 275.
[28] A. V. Volkov, K. Wijeratne, E. Mitraka, U. Ail, D. Zhao, K. Tybrandt, J. W. Andreasen, M. Berggren, X. Crispin, I. V. Zozoulenko, *Adv. Funct. Mater.* **2017**, *27*, 1700329.
[29] C. M. Proctor, J. Rivnay, G. G. Malliaras, *J. Polym. Sci., Part B Polym. Phys.* **2016**, *54*, 1433.
[30] V. I. Arkhipov, P. Heremans, E. V. Emelianova, G. J. Adriaenssens, H. Bässler, *Appl. Phys. Lett.* **2003**, *82*, 3245.
[31] M. Yamashita, C. Otani, H. Okuzaki, M. Shimizu, *30th URSI Gen. Assem. Sci. Symp.* **2011**, *1*, 3.
[32] T. Uemura, C. Rolin, T. H. Ke, P. Fesenko, J. Genoe, P. Heremans, J. Takeya, *Adv. Mater.* **2016**, *28*, 151.
[33] M. Nikolou, G. G. Malliaras, *Chem. Rec.* **2008**, *8*, 13.
[34] K. Tybrandt, I. V. Zozoulenko, M. Berggren, *Sci. Adv.* **2017**, *3*, 12.
[35] L. Groenendaal, F. Jonas, D. Freitag, H. Pielartzik, J. R. Reynolds, *Adv. Mater.* **2000**, *12*, 481.
[36] M. Tsuno, M. Suga, M. Tanaka, K. Shibahara, M. Miura-Mattausch, M. Hirose, *IEEE Trans. Electron Devices* **1999**, *46*, 1429.
[37] P. V. Pesavento, R. J. Chesterfield, C. R. Newman, C. D. Frisble, *J. Appl. Phys.* **2004**, *96*, 7312.
[38] B. Charlot, G. Sassine, A. Garraud, B. Sorli, A. Giani, P. Combette, *Microsyst. Technol.* **2013**, *19*, 895.

© 2021 The Authors. Advanced Electronic Materials published by Wiley-VCH GmbH